POLITECNICO DI TORINO
Repository ISTITUZIONALE

Graphene Oxide Membranes for Critical Raw Materials Recovery and Water Purification: From Cleanroom Wastewater to Fluorite

Original
Graphene Oxide Membranes for Critical Raw Materials Recovery and Water Purification: From Cleanroom Wastewater to Fluorite / Pedico, A., Stanzione, F., Romaniello, F., Astorino, C., Berruto, M., Landi, G., Rossi, A.M., Bocchini, S., Calonico, D.. - In: ADVANCED ENERGY AND SUSTAINABILITY RESEARCH. - ISSN 2699-9412. - 7:9(2026), pp. 1-10. [10.1002/aesr.70255]

Availability:
This version is available at: 11583/3015260 since: 2026-09-07T09:51:06Z

Publisher:
Wiley

Published
DOI:10.1002/aesr.70255

Terms of use:

This article is made available under terms and conditions as specified in the corresponding bibliographic description in the repository

Publisher copyright

(Article begins on next page)

08 October 2026

Advanced Energy and Sustainability Research

ADVANCED ENERGY & SUSTAINABILITY RESEARCH Open Access

www.advenergysustres.com

RESEARCH ARTICLE OPEN ACCESS

Graphene Oxide Membranes for Critical Raw Materials Recovery and Water Purification: From Cleanroom Wastewater to Fluorite

Alessandro Pedico[1,2] | Fernando Stanzione[3] | Francesco Romaniello[1] | Carmela Astorino[2,4] | Matteo Berruto[1] | Gianluca Landi[3] | Andrea Mario Rossi[1] | Sergio Bocchini[2,4] | Davide Calonico[1]

[1]Istituto Nazionale di Ricerca Metrologica, Torino, Italy | [2]Dipartimento di Scienza Applicata e Tecnologia (DISAT), Politecnico di Torino, Torino, Italy | [3]Consiglio Nazionale delle Ricerche, Istituto di Scienze e Tecnologie per l'Energia e la Mobilità Sostenibili, Napoli, Italy | [4]Center for Sustainable Future Technologies, Istituto Italiano di Tecnologia, Torino, Italy

Correspondence: Alessandro Pedico (a.pedico@inrim.it)

Received: 9 April 2026 | **Revised:** 22 July 2026 | **Accepted:** 17 August 2026

Keywords: circular economy | critical raw material | fluorite | graphene oxide | water purification

ABSTRACT

The European Union has identified fluorite (CaF_2) as a critical raw material (CRM) due to its economic importance, negligible recycling, and high import dependency. This study investigates a functionalized graphene oxide (fGO) membrane for purifying wastewater containing dissolved fluorides below the solubility limit of CaF_2 and the subsequent CRM recovery. While the fundamental interaction is known in batch systems, closed-loop recovery processes using this kind of membrane remain unexplored. Utilizing fGO synthesized via a scalable, green approach, we transition beyond conventional adsorption to a dynamic membrane-stripping cycle. Comprehensive material characterization is provided. The fGO membranes were tested in a real-case scenario using cleanroom facility wastewater. Fluorine concentration was successfully reduced from 21 down to 1.4 mg L^{-1}, meeting the EU/USA discharge and drinking water standards. High-purity CaF_2 powder was recovered. This work establishes a viable, non-conventional membrane-based approach for waste valorization, advancing circular economy principles in the semiconductor and microelectronics industries by transforming a hazardous waste into a strategic resource.

1 | Introduction

The concept of critical raw materials (CRMs) has gained significant global attention, particularly within the European Union (EU) due to their high economic importance and significant supply risk. These materials are essential for industrial value chains and strategic sectors, including renewable energy, digital technologies, and defense. The European Commission regularly publishes its list of CRMs, accompanied by the EU Critical Raw Materials Act (a legislative framework outlining definitions, projects, initiatives, and regulations) [1]. The list of CRMs highlights potential vulnerabilities and encourages sustainable sourcing and resource efficiency. Among these materials, fluorite (or fluorspar), a mineral composed of calcium fluoride (CaF_2), has been on this list since its very first release in 2011 and has never left it. Fluorite is a crucial industrial mineral with diverse applications, ranging from the production of hydrofluoric acid, a precursor for many fluorine-containing chemicals, to its use as a flux in aluminum, iron, and steel making and in the manufacture of enamels and optical lenses. Observing the trend of this CRM over the years, its import in the EU slightly decreased (69% in 2011 [2], 70% in 2017 [3], 66% in 2020 [4], and 60% in 2023 [5]), while the recycling rate barely increased from 0% to 1% over a decade. The EU's reliance on imports of fluorite, coupled with its indispensable role in key industries, underlines the urgency of developing alternative sources and recovery strategies, with particular focus on recycling methods, which are currently lacking.

This is an open access article under the terms of the Creative Commons Attribution License, which permits use, distribution and reproduction in any medium, provided the original work is properly cited.

© 2026 The Author(s). *Advanced Energy and Sustainability Research* published by Wiley-VCH GmbH.

While the sources of fluorite are primarily minerals and related extraction activities, the sources of fluorides are less limited. Chemical industries, metallurgical industries, glass manufacturers, and cleanroom facilities, especially those involved in semiconductor manufacturing or related high-tech industries, often generate wastewater streams containing significant concentrations of fluoride ions. The discharge of such effluents is strictly regulated due to the potential adverse health effects of excessive fluoride intake, with national and international regulations imposing stringent limits on fluoride concentrations in drinking water and environmental discharges. For drinking water, USA sets this limit to 4.0 mg L^{-1}, while the EU set this value at 1.5 mg L^{-1} [6]. Therefore, the recovery of fluorine from these waste streams, rather than its mere removal and disposal, presents an attractive opportunity. Specifically, the recovered fluoride can be converted into CaF_2, effectively regenerating the CRM. This approach not only mitigates environmental pollution but also aligns perfectly with the principles of a circular economy, promoting waste reutilization and reducing the reliance on primary resource extraction.

The conventional method for converting fluoride in CaF_2 is based on the precipitation of CaF_2, obtained by adding calcium-containing chemicals to the fluorine-rich solution and exploiting the poor solubility of CaF_2 in water (17 mg L^{-1} at 20 °C, corresponding to about 8 mg L^{-1} of fluoride at 20 °C), which is extremely low compared to other fluorides like sodium fluoride (42 g L^{-1} at 20 °C). The solution can then be filtered, and the precipitate recovered. However, this method, while being simple and effective, cannot reduce the concentration of fluorides down to 1.5 mg L^{-1} as required for safe discharge of wastewater or drinking water in the EU, with this target being about 6 times lower than the solubility limit. To achieve this sub-solubility polishing, conventional industrial frameworks often rely on purely extractive technologies such as activated alumina, ion exchange resins, or reverse osmosis (RO). While these methods can successfully drive residual fluoride concentrations down to permissible discharge limits, they generate highly concentrated, complex secondary waste streams rather than facilitating resource recovery. Consequently, a critical technological gap remains: a system capable of bridging the deficit between stringent environmental compliance and high-purity mineral circularity. For this reason, it is necessary to investigate new and efficient ways to further reduce the concentration of fluorides in water below the solubility limit while contemporaneously recovering such a precious resource.

Traditional water treatment and resource recovery technologies, such as standard nanofiltration membranes, often face limitations in terms of selectivity, fouling, and chemical resistance [7, 8]. In recent years, graphene oxide (GO) membranes have emerged as a promising alternative, offering several advantages. These membranes, made of a stack of two-dimensional GO nanosheets, possess unique properties including high water permeability, tunable interlayer spacing for precise molecular sieving, excellent mechanical strength, and antifouling characteristics [9, 10]. The selectivity of GO membranes is primarily governed by the synergy between electrostatic interactions and physical confinement. Donnan exclusion plays a crucial role when charged species are present in the solution. The negatively charged functional groups on the GO surface create an electrostatic barrier that repels co-ions, making the GO membranes good candidates as cation-exchange membranes [11]. Simultaneously, the interlayer distance between GO nanosheets acts as a sub-nanometer sieve. By tuning this spacing to approximate the hydrated radii of target ions, the membrane can effectively discriminate between species that would otherwise exhibit a similar chemical behavior [12]. Furthermore, these membranes can be produced through scalable and green methods [13]. Finally, these membranes find their ideal application in dead-end filtration systems, highly desirable thanks to their operational simplicity and low energy consumption of the order of 10^{-1} kWh m^{-3}, one order of magnitude lower than that of reverse osmosis systems (thanks to the lower applied pressure) and two orders of magnitude lower than thermal evaporation processes (the filtration is performed at ambient temperature) [14]. These characteristics make GO membranes a good candidate for challenging separation processes, potentially overcoming the drawbacks associated with conventional polymeric or ceramic membranes (Table S1).

In the field of raw material recovery, GO membranes are reported for their efficacy in lithium recovery from water sources, a CRM well known for energy storage applications [15–17]. However, the application of these membranes for other specific CRMs, like fluorite, remains largely unreported. One area where the advanced separation capabilities of GO membranes can be particularly impactful is in the recovery of fluorine from industrial wastewater. While literature exists on composite materials containing GO [18] or static batch adsorption [19], no studies have yet tested and engineered GO membranes for a circular recovery cycle of fluorite, nor addressed the engineering challenges of a continuous recovery process. By transforming a dangerous waste into a valuable product, the application of GO membranes for fluorine recovery can contribute to a more sustainable and resource-efficient industrial ecosystem, bridging the gap between wastewater remediation and sustainable resource management.

This study demonstrates a closed-loop system utilizing functionalized graphene oxide (fGO) membranes specifically tailored to overcome the limitations of both conventional chemical precipitation and standard extractive technologies. By targeting the residual fluoride fraction that escapes standard precipitation, this system achieves a distinct quantitative dual advantage that traditional alternatives (like reverse osmosis, activated alumina, or ion exchange resins) do not readily offer: the simultaneous achievement of high-purity CaF_2 recovery and the reduction of effluent fluoride retention to strictly below the EU drinking water limit of 1.5 mg L^{-1}. Tailored for the recovery of fluoride ions from real cleanroom wastewater, this approach aimed at closing the loop on fluorite utilization. The fGO is produced following a refined, scalable, and green methodology, based on a modification of a method we described previously [20]. This approach offers a key advantage over traditional, environmentally impactful solvent-based membrane synthesis. A quaternary ammonium methacrylate derivative was selected for functionalization to target fluoride ions. The permanent positive charge of the ammonium moiety creates localized anion-exchange sites within the fGO channels, facilitating fluoride transport and capture through strong electrostatic attraction. The performance of different GO membranes is compared using a set of artificial solutions to test their selectivity for fluoride ions under various conditions. Selectivity and recovery rate as a function of the concentration

26999412, 2026, 9, Downloaded from https://advanced.onlinelibrary.wiley.com/doi/10.1002/aesr.70255 by Iit Istituti Italiano Di Tecnologia, Wiley Online Library on [07/09/2026]. See the Terms and Conditions (https://onlinelibrary.wiley.com/terms-and-conditions) on Wiley Online Library for rules of use; OA articles are governed by the applicable Creative Commons License

of fluorides and competing anions are reported, together with a real-case study of defluorination of wastewater from a cleanroom facility.

2 | Material and Methods

2.1 | Solutions Preparation

Solutions at different concentration of sodium fluoride (≥99% purity, Thermo Scientific), sodium chloride (≥99% purity, Fisher BioReagents), sodium sulfate (anhydrous, ≥99% purity, Thermo Scientific), sodium phosphate monobasic (anhydrous, ≥99% purity, Fisher BioReagents), sodium hydroxide (anhydrous, ≥98% purity, Merck), calcium hydroxide (≥98% purity, Thermo Scientific), and calcium chloride (dihydrate, ≥99% purity, Thermo Scientific) have been prepared dissolving the salts in deionized water (Milli-Q IQ 7000, Merck Millipore).

2.2 | Functionalized Graphene Oxide

In this new functionalization procedure of the GO sheets, we dedicated significant effort on improving the sustainability of the process we previously reported [20], strongly reducing the energy consumption of the UV radiation source (from a 500 W lamp with an irradiance of 2 kW m^{-2} down to a 6 W led with an irradiance of 0.35 kW m^{-2}, keeping the same exposure time) and substituting the N,N-dimethylformamide (an hazardous, environmental persistent, non-green solvent widely used in industrial processes) with water and dimethyl isosorbide, a biodegradable, non-hazardous, green solvent derived from D-sorbitol, obtained from biomasses (renewable feedstock). Also, we substituted 4-hydroxybenzophenone with 2-hydroxybenzophenone (its less hazardous counterpart) and the (2-(acryloyloxy)ethyl)trimethylammonium chloride with 2-(methacryloyloxy)ethyltrimethylammonium chloride (a similar but more stable and less hazardous reagent).

Briefly, commercial GO dispersion (2% w/w in H_2O, >95% monolayer, 14–17 μm lateral size, Graphenea) is diluted with dimethyl isosorbide (DMI, ≥99% purity, Merck) to a concentration of 2 g L^{-1}. Then, 2-hydroxybenzophenone (HBP, 99% purity, Thermo Scientific) is added to the dispersion in an amount triple with respect to the mass of GO. The dispersion obtained in this way was stirred for 15 min. At this point, it was exposed to UV radiation (365 nm MicroBrite LED, Advanced Illumination) for 5 min with an intensity of 350 W m^{-2} while stirring. After this treatment, the result is GO functionalized with HBP. Subsequently, the dispersion was centrifuged (R-10M, REMI) at 4000 rpm for 30 min. The precipitate was washed in ethanol (anhydrous, ≥99.5% purity, Merck) and centrifuged. This step was repeated 3 times to separate the unreacted material. The fGO obtained in this way (fGO-Step I) is dispersed again in DMI in a concentration of 2 g L^{-1}. To achieve the final desired functionalization, the proper amount of 2-(methacryloyloxy)ethyltrimethylammonium chloride solution (72% in H_2O, Thermo Scientific) is added to the dispersion in the ratio 5:1 with respect to fGO-Step I. The solution is exposed to UV, centrifuged, and washed again. The only difference is that the exposure time was 15 min in this case. After the final washing, fGO-Step II is obtained, and it is stored in ethanol in a concentration of 5 g L^{-1}. A visual representation of the functionalization procedure is provided in the Supporting Information (Figure S1).

2.3 | Membrane Fabrication

GO membranes were fabricated using a pressure-assisted method. A commercial polymeric support made of polyethersulfone (PES, Ø 47 mm, nominal pore size 100 nm, Sterlitech) was placed at the bottom of a dead-end filtration apparatus (HP4750, Sterlitech). A GO solution is poured into the cell, and pressure is applied to it from the top by means of compressed air. The solution is forced to pass through the polymeric support, while the GO sheets accumulate on the surface of the polymer, forming the typical GO membrane-stacked structure. The process is stopped once all the solution is passed through the support. The membranes obtained in this way have a diameter of 38 mm (an area of 11.34 cm^2) and a mass loading of 0.18 mg cm^{-2} (2 mg of GO per membrane).

Three different types of membranes were produced following the procedure described above: pure GO membranes, obtained by diluting the commercial GO dispersion with deionized H_2O down to a concentration of 0.05 g L^{-1}; Ca-rich GO membranes, obtained by diluting the commercial GO dispersion with a 10 mM $CaCl_2$ solution down to a concentration of 0.05 g L^{-1} and stirred for 1 h before use; and fGO membrane, obtained by diluting the fGO-step II dispersion with deionized H_2O down to a concentration of 0.05 g L^{-1}.

2.4 | Characterization Techniques

Electron microscopy characterization was carried out with a field-emission scanning electron microscope (FESEM Supra 40, manufactured by Zeiss) equipped with a Si(Li) detector (Oxford Instruments) for energy-dispersive X-ray (EDX) spectroscopy.

X-ray diffraction (XRD) spectroscopy (X'Pert pro, Malvern Panalytical) was employed to measure the interlayer distance between GO sheets in the stacked membranes and to check the purity of the recovered CaF_2. The instrument was set to work with a Bragg–Brentano configuration, exploiting a Cu-K source with $\lambda = 1.541874$ Å. The measurements were performed with a step size of 0.026° at a scan speed of 200 s $step^{-1}$.

Thermogravimetric analysis (TGA) was performed on approximately 2 mg of the sample using a TG 209 F1 Libra thermobalance (NETZSCH GmbH). Samples were heated from 25 to 800 °C at a constant rate of 20 °C min^{-1} under a nitrogen flow of 40 cm^3 min^{-1}. The experimental mass error was typically below 0.05 mg (corresponding to approximately ±2.5%).

Evolved gas analysis was carried out using a TGA-FTIR setup. Gas-phase IR spectra were acquired using a Bruker Tensor II spectrometer equipped with a gas cell maintained at 200 °C to prevent condensation of degradation products. The TGA instrument and the FTIR spectrometer were coupled via a heated transfer line (230 °C) using a NETZSCH FT-IR Coupling System. Prior to analysis, the transfer line was cleaned with three cycles of evacuation and nitrogen refill to ensure a stable IR background.

26999412, 2026, 9, Downloaded from https://advanced.onlinelibrary.wiley.com/doi/10.1002/aesr.70255 by Iit Istituti Italiano Di Tecnologia, Wiley Online Library on [07/09/2026]. See the Terms and Conditions (https://onlinelibrary.wiley.com/terms-and-conditions) on Wiley Online Library for rules of use; OA articles are governed by the applicable Creative Commons License

Infrared spectra of the evolved gases were recorded at intervals of approximately 3 °C (about every 10 s).

Fourier transform infrared (FTIR) spectroscopy (Bruker Tensor II) was performed on the material in attenuated total reflection (ATR) configuration.

Z-potential was measured by a Litesizer DLS 500 (Anton Paar) on solutions with a concentration of 0.1 g L^{-1}.

The residual anion concentration after the filtration tests was measured using ion chromatography. The analyses were carried out using a Metrohm 883 IC Basic Ion Chromatograph with chemical suppression; the column used for the separation of the different anions was a Metrosep A Supp 5 – 250/4.0. The system was previously calibrated with certified standard solutions.

Elemental analysis–isotope ratio mass spectrometry (EA-IRMS) was performed using a Thermo Scientific FlashSmart Elemental Analyzer operated in the oxidative mode. Approximately, 1 mg of each sample was weighed into tin capsules and combusted at 1020 °C. Analyses were carried out in quintuplicate on GO before and after functionalization.

Elemental impurities in the recovered salt were determined by high-resolution inductively-coupled plasma mass spectrometry (ICP-MS) using a Thermo Scientific Element ICP-HRMS. Approximately 100 mg of sample was weighed and digested with 8 ml of 68% HNO_3 in a microwave digestion system. The digestion program consisted of a 15 min ramp to 200 °C, followed by a 15 min hold at 200 °C, and subsequent cooling. Scandium was added as an internal standard before digestion in order to monitor both instrumental drift and possible anomalies occurring during sample preparation. After digestion, the solution was diluted to 50 ml; then, 3.15 ml of this solution was further diluted to 10 ml prior to multi-element quantitative ICP-MS analysis.

Raman spectroscopy was performed using a DXR Raman Microscope (Thermo Fisher Scientific) operating in the high-resolution mode (spectral resolution of 5 cm^{-1}) using a 532 nm laser operating at 6 mW. Data acquisition was performed using OMNIC software, setting an acquisition time of 30 s.

2.5 | Filtration Tests

Filtration tests were performed in the same dead-end apparatus used for membrane fabrication (Figure S2). If not stated otherwise, the applied pressure is 1 bar, and the feed volume is 50 ml (40 ml for stripping solutions). Between different tests, the apparatus was carefully washed with abundant deionized H_2O and dried with compressed air in order to prevent any contamination. Each filtration test was repeated 3 times for repeatability purposes.

The retention is evaluated as 1 minus the fraction of the target ion detected in the permeate. The recovery was evaluated as the fraction of the target ion detected in the stripping solution. Both are reported as percentages.

3 | Results and Discussion

3.1 | Material Characterization

Z potential measurements (Figure 1a) performed on GO and fGO show how the functionalization impacted the surface charge of the material, moving from −23 mV for pristine GO to +11 mV for fGO. The potential shift is linked to the reduction of oxygen functional groups (negatively charged in water) and the addition of positively charged amine groups. ATR–FTIR spectroscopy analysis (Figure 1b) highlights the progressive modification of GO through sequential functionalization. The spectrum of pristine GO was compared with those of two functionalized samples, obtained after the incorporation of 2-hydroxybenzophenone (fGO-Step I) and the subsequent introduction of a quaternary ammonium methacrylate derivative (fGO-Step II), as described in the Experimental section.

The spectrum of GO (black line in Figure 1) exhibits a vibrational profile typical of oxidized graphene materials, in agreement with the literature [21–23]. A broad band centered around

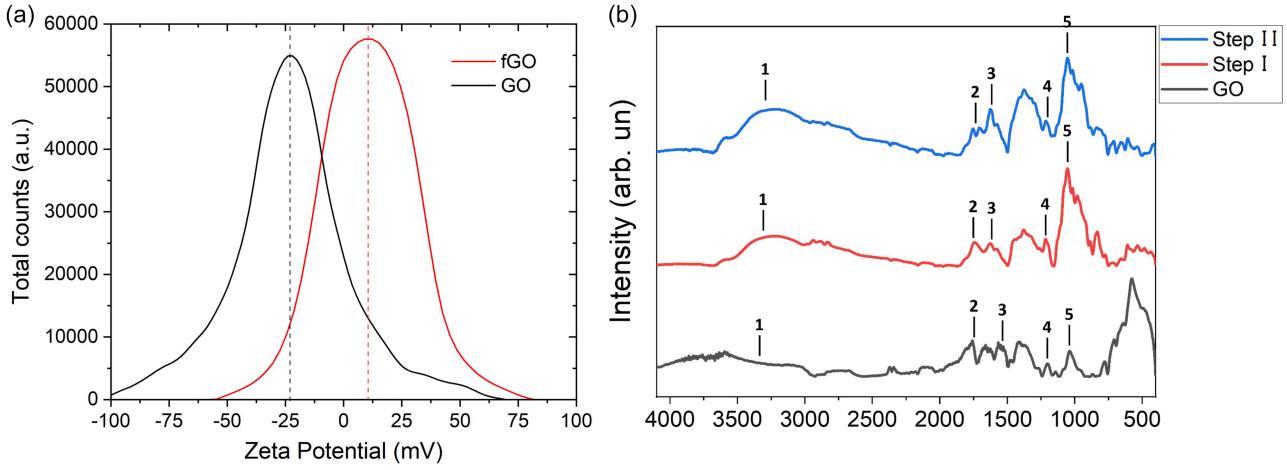

FIGURE 1 | (a) *Z* potential measurements on GO and fGO. (b) ATR–FTIR spectra of graphene oxide (GO, black), functionalized GO after reaction with 2-hydroxybenzophenone (fGO–Step I, red), and after subsequent modification with a quaternary ammonium methacrylate derivative (fGO–Step II, blue).

26999412, 2026, 9, Downloaded from https://advanced.onlinelibrary.wiley.com/doi/10.1002/aesr.70255 by Iit Istituti Italiano Di Tecnologia, Wiley Online Library on [07/09/2026]. See the Terms and Conditions (https://onlinelibrary.wiley.com/terms-and-conditions) on Wiley Online Library for rules of use; OA articles are governed by the applicable Creative Commons License

3400 cm^{-1} (1) is assigned to O—H stretching vibrations from the hydroxyl and carboxylic acid groups. A sharp absorption at 1760 cm^{-1} (2) corresponds to the C═O stretching of carboxylic acids, predominantly located at the edges of GO sheets [21, 23, 24]. The signal at 1630 cm^{-1} (3) arises from C═C stretching vibrations of the conjugated carbon framework in the graphene lattice [21, 23]. The band at 1200 cm^{-1} (4) is attributed to C—OH stretching, while the absorption at 1039 cm^{-1} (5) corresponds to C—O—C vibrations of epoxy functionalities, indicative of GO oxidation [21, 23, 25].

Upon HBP addition (red line), new spectral features emerge, suggesting a successful interaction or covalent incorporation. A slight shift of the C═O stretching band (2) toward lower wavenumbers is observed, reflecting the contribution of the aromatic ketone group in HBP [26]. The broader band around 1600 cm^{-1} (3) is likely due to overlapping C═C stretching vibrations from both GO and the aromatic rings of HBP [26]. Furthermore, the C—O stretching vibration of the phenolic hydroxyl in HBP contributes to the intensified band near ~1050 cm^{-1} (5) [26]. Finally, a structural reorganization of graphene oxide is observed, indicative of a photoreduction process or a rearrangement of the carbon framework. The disappearance of IR bands in the 1000–600 cm^{-1} region can be attributed to the loss of oxygen-containing functional groups (such as C—O, epoxides, and alcohols), promoted by the photosensitizing action of benzophenone. This suggests a partial transition toward more aromatic and less functionalized structures, consistent with rGO [27].

The final spectrum (blue line), corresponding to the introduction of the quaternary ammonium compound, shows additional complexity. An increase in absorption is observed in the high-wavenumber region (~3000–3500 cm^{-1}), attributed to O—H and C—H stretching vibrations (1). The band near 1700 cm^{-1} (2), assigned to carbonyl stretching, is more intense in pristine GO, and its intensity decreases in Step I and further in Step II, indicating a partial consumption or transformation of carboxylic/ester groups during the two-step functionalization. In contrast, the band around 1600 cm^{-1} (3) becomes relatively more prominent in the final spectrum, which can be ascribed to overlapping C═C stretching vibrations from the methacrylate moiety and the aromatic domains of the GO/HBP framework. Finally, a broad and intensified band in the 1100 cm^{-1} region (5) is consistent with C—O/C—N stretching modes associated with the quaternary trimethylammonium methacrylate units [28].

These spectral changes confirm the progressive functionalization and structural evolution of the GO-based membrane through a two-step chemical modification process.

TGA was performed to assess the thermal stability of the samples and to further confirm the progressive functionalization of GO. The thermogravimetric (TG) and derivative thermogravimetric (DTG) curves of the fGO membranes are presented in Figure 2. To support the interpretation of each weight loss event, the corresponding FTIR spectra of the evolved gases are provided in the Supporting Information.

An initial weight loss of approximately 5% is observed for GO in the temperature range of 55–135 °C, which is attributed to the release of physically adsorbed water on the hydrophilic GO surface [29]. This weight loss is also evident in fGO–Step II, where FTIR analysis of the evolved gases indicates, in addition to water, the presence of CO_2 (Figure S3). The DTG peak corresponding to this event is centered at 87 °C. Interestingly, in fGO–Step I, the weight loss in this region is significantly lower compared to pristine GO, suggesting a partial loss of surface hydrophilicity. This observation is consistent with the partial removal or transformation of oxygenated functional groups, likely due to side reactions occurring during the first functionalization step.

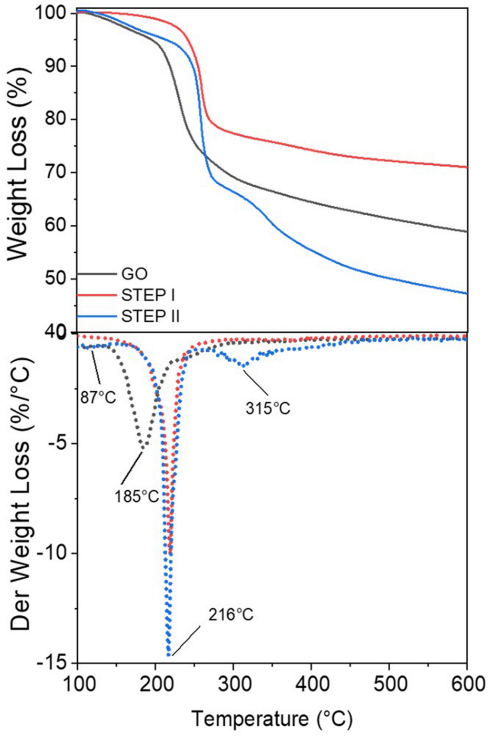

FIGURE 2 | TGA and DTGA curves of graphene oxide (GO, black), GO functionalized with 2-hydroxybenzophenone (fGO–Step I, red), and GO further modified with a quaternary ammonium methacrylate derivative (fGO–Step II, blue).

As the temperature increases from 150 to 230 °C, GO undergoes a significant weight loss of approximately 28%, with a DTG peak centered at 185 °C. This step is attributed to the thermal decomposition of oxygen-containing functional groups, particularly carboxylic (—COOH) and carbonyl (C═O) moieties, which evolve as H_2O, CO_2, and CO. This interpretation is supported by the FTIR analysis of the released gases (Figure S4).

Further weight loss occurs at approximately 216 °C as evidenced by a DTG peak at this temperature. This thermal event results in a 23% mass loss in fGO–step I and increases to approximately 32% in fGO–Step II. It is similarly attributed to the decomposition of residual carboxylic and carbonyl groups, as confirmed by the presence of CO_2 and CO in the evolved gas spectra (Figure S5) [20]. The lower mass loss observed for fGO–Step I relative to GO in this temperature range further supports the interpretation that some of the native oxygen functionalities were already removed or chemically altered during the first functionalization step.

Finally, a distinct weight loss of about 14% is observed exclusively in the fGO–Step II sample at around 305 °C. FTIR analysis of the

26999412, 2026, 9, Downloaded from https://advanced.onlinelibrary.wiley.com/doi/10.1002/aesr.70255 by Iit Istituti Italiano Di Tecnologia, Wiley Online Library on [07/09/2026]. See the Terms and Conditions (https://onlinelibrary.wiley.com/terms-and-conditions) on Wiley Online Library for rules of use; OA articles are governed by the applicable Creative Commons License

evolved gases reveals two new absorption bands corresponding to trimethylamine (TMA) and hydrogen chloride (HCl), indicating the thermal decomposition of the quaternary ammonium moiety introduced during the second functionalization step (Figure S6) [20].

Nitrogen EA-IRMS on pristine GO showed a non-determinable nitrogen content, whereas the post-grafting material exhibited an average nitrogen content of 0.1063 ± 0.0070 % w/w, corresponding to 0.00106 ± 0.00007 mg of N per mg of fGO. The detection of nitrogen only after grafting supports the successful introduction of nitrogen-containing quaternary amine groups onto the fGO surface.

Raman spectra of GO and fGO were collected to further investigate the structural changes following functionalization (Figure S7). Pristine GO exhibited an I_D/I_G intensity ratio of 0.95, which decreased to 0.83 for fGO. The G band showed a slight downshift towards 1580 cm^{-1}. These combined effects demonstrate a decreased oxygen defect density and enhanced structural ordering of the carbon lattice, confirming that functionalization proceeded alongside a partial reduction, without introducing additional structural defects [30].

Electron microscopy was employed to check the uniformity of the GO membranes (Figure 3). No appreciable difference was observed between the different samples in terms of superficial roughness. On the contrary, a different thickness was observed. GO membranes have a thickness of 0.8–1.0 µm, while Ca-rich GO membranes have a thickness of only 0.6–0.8 µm and fGO membranes have a thickness of 1.0–1.2 µm. These values are easily explained by considering the effect of the addition of Ca^{2+} ions (like many other cations), which are known in the literature to be responsible for shrinking the structure of the membrane and improving its compactness [31]. Accordingly, fGO is expected to

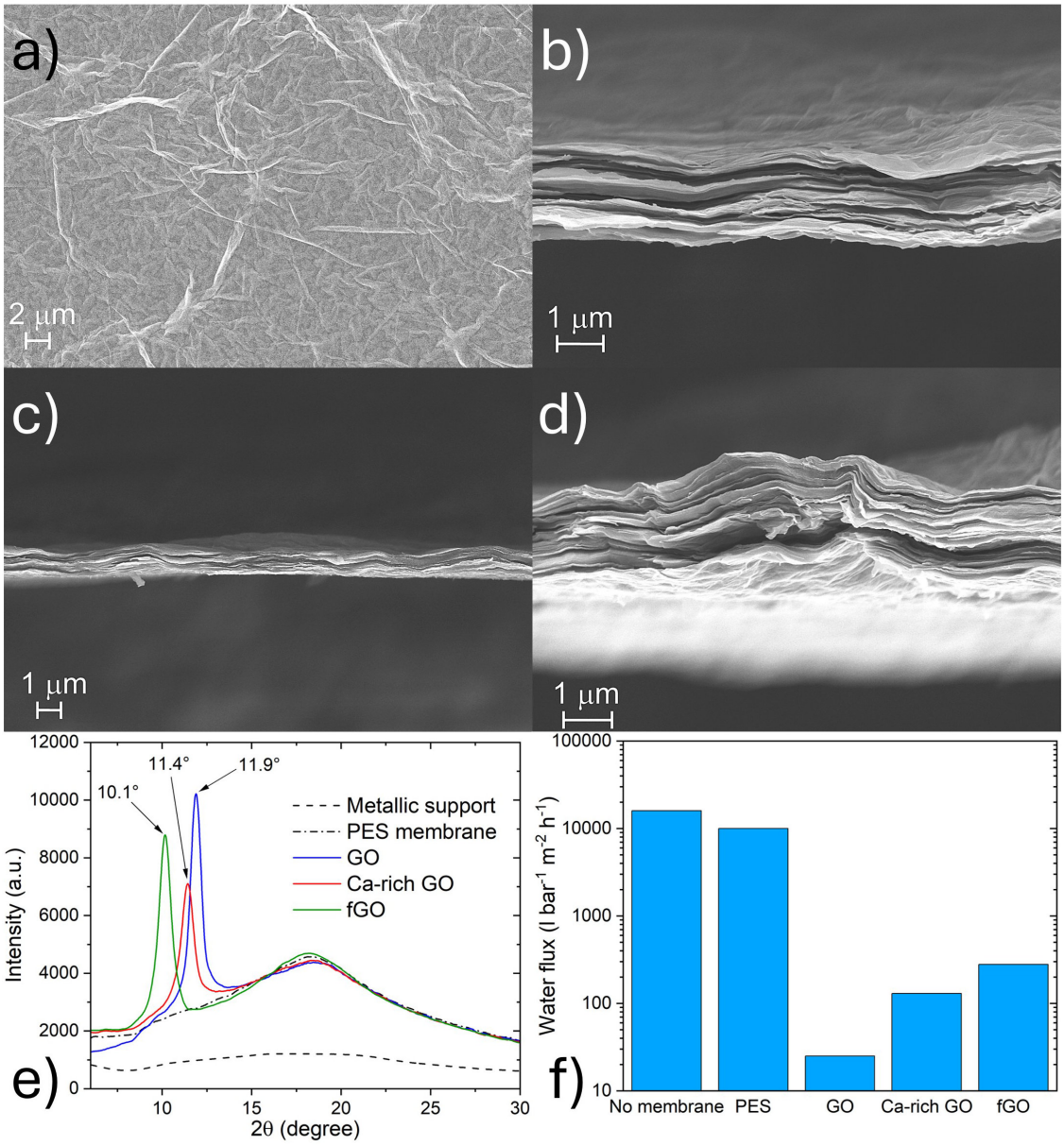

FIGURE 3 | (a) Top view of a fGO membrane. (b) Cross section of a Ca-rich GO membrane. (c) Cross section of a GO membrane. (d) Cross section of a fGO membrane. (e) XRD patterns of the different membranes and supports. (f) Water flux comparison of different membranes.

26999412, 2026, 9, Downloaded from https://advanced.onlinelibrary.wiley.com/doi/10.1002/aesr.70255 by Iit Istituti Italiano Di Tecnologia, Wiley Online Library on [07/09/2026]. See the Terms and Conditions (https://onlinelibrary.wiley.com/terms-and-conditions) on Wiley Online Library for rules of use; OA articles are governed by the applicable Creative Commons License

be thicker than GO due to the presence of the functional monomer on the surface of the GO sheets, which is also reported in the literature to be a strategy to increase and control the interlayer distance between the GO sheets [32].

XRD analysis (Figure 3e) performed on dried membranes confirmed that the smallest interlayer distance is observed in the GO membranes (0.75 nm), which increases in the case of the Ca-rich GO membranes (0.78 nm) due to the presence of Ca^{2+} ions inside the channels. As expected, the grafting of a polymeric monomer on the surface of the GO flakes translated into the observation of the largest interlayer distance (0.87 nm) in the case of fGO. Due to the small thickness of these membranes, the broad amorphous peak of the PES support is clearly visible in all samples (centered around 18°).

The water flux was evaluated for all membranes using deionized H_2O. The results are reported in Figure 3f. The impact of the PES support was totally negligible. The water flux of GO membranes was the lowest, being one order of magnitude lower than that of Ca-rich GO and fGO membranes. Among them, fGO showed the highest flux, reaching almost 300 L bar^{-1} m^{-2} h^{-1}. The water uptake was evaluated by weight. The membranes were dried at 40 °C overnight under low-vacuum conditions inside a glass oven (B-585, Büchi). Afterwards, they were immersed in deionized water for 2 h and then gently dried using lint-free paper and immediately weighed. GO membranes showed a water uptake of 40% of their dried weight compared to 25% for the fGO membranes. PES support alone showed a water uptake of 20%.

3.2 | Filtration Tests

The first set of filtration tests was performed in order to compare the selectivity of the different membranes towards fluorides. To do so, a NaF 22 mg L^{-1} solution (F^- 10 mg L^{-1}) was employed. The solution was passed through the apparatus first and then filtered using a PES membrane. Samples were collected and analyzed for both cases in order to exclude any possible adsorption from the apparatus or from the PES membrane. IC analysis confirmed that the NaF feed solution and those samples had the same fluoride concentration. After that, the NaF solution was filtered through 3 different membranes (GO, Ca-rich GO, and fGO). After each permeate collection, a 0.1 M NaOH stripping solution was filtered. This solution was used to collect the fluoride ions trapped inside the membrane and substite them with hydroxide ions. This process was repeated 3 times for each membrane using the same solutions, thus reducing the concentration of fluorides in the permeate after each filtration while increasing its concentration in the stripping solution. IC analysis performed on both permeates and stripping solutions is reported in Figure 4a. The results indicate good reproducibility in terms of retention but more variability for the recovery, with the exception of the Ca-rich GO. We suppose that stable recovery in this specific case is due to the presence of the calcium ions, which effectively prevent the channels from widening under wet conditions [31] while simultaneously providing preferential sites for fluoride adsorption. Furthermore, NaOH amplifies this effect by weakening the hydrogen bonds responsible for the stability of the stacked structure of these membranes. As a result of this first set of tests, fGO was selected as the best-performing material. It exhibited the highest retention, slightly higher than GO. It also exhibited the highest recovery, being slightly higher than that of Ca-rich GO. To further confirm the mechanism of fluorine removal, EDX analysis was performed on the fGO membranes after the tests, which revealed no detectable trace of fluorine. This result is consistent with a reversible adsorption mechanism, providing evidence of the stripping effectiveness of the NaOH solution. This is evidence that the quaternary amine grafted on the surface of the GO sheets can enhance the affinity for fluorides without creating sites in which the fluorine ions become permanently trapped.

The second set of experiments was performed in order to test the selectivity of fGO toward fluorides (Figure 4b). Indeed, the presence of positively charged monomers containing quaternary amines on the surface of the fGO sheets does not imply selectivity towards specific anions. For this reason, a set of solutions containing the same cation (Na^+) but different anions were prepared. Two solutions of NaF, 22 and 550 mg L^{-1} (F^- 10 and 250 mg L^{-1}, respectively), two solutions of NaCl, 16.5 and 410 mg L^{-1} (Cl^- 10 and 250 mg L^{-1}, respectively), a solution of Na_2SO_4, 375 mg L^{-1} (SO_4^{2-} 250 mg L^{-1}), a solution of NaH_2PO_4, 315 mg L^{-1} (PO_4^{3-} 250 mg L^{-1}), and a mixed solution containing 50 mg L^{-1} of each anion were used as feed solutions. The stripping solution was always 0.1 M NaOH. Feed and stripping solutions were filtered twice each on the same fGO membrane. Different

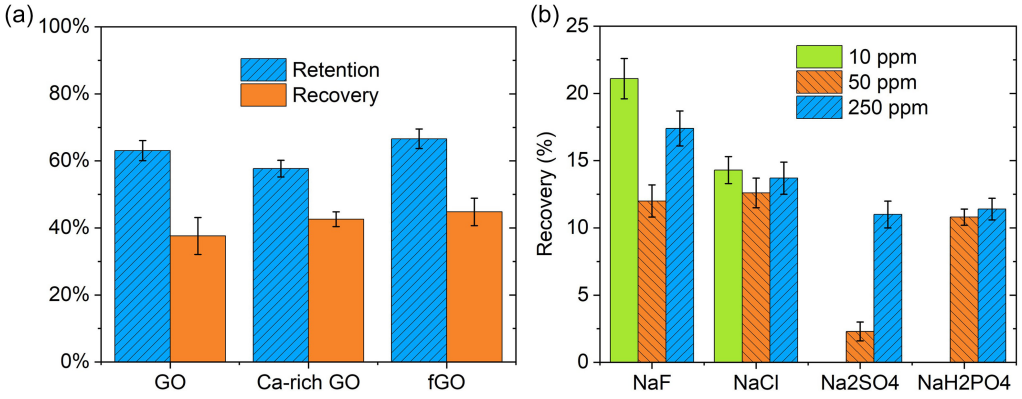

FIGURE 4 | (a) Comparison of different membranes. The solution is NaF 22 mg L^{-1}. (b) Recovery rate of fGO membranes. The concentration in the legend refers to the anions.

26999412, 2026, 9, Downloaded from https://advanced.onlinelibrary.wiley.com/doi/10.1002/aesr.70255 by Iit Istituti Italiano Di Tecnologia, Wiley Online Library on [07/09/2026]. See the Terms and Conditions (https://onlinelibrary.wiley.com/terms-and-conditions) on Wiley Online Library for rules of use; OA articles are governed by the applicable Creative Commons License

membranes were used for each feed composition to avoid any contamination. The results show that at a concentration of 250 mg L^{-1}, the selectivity is higher for fluorides rather than the other anions. Notably, the recovery rates of sulfates and phosphates are comparable, while the chlorides are slightly higher. At 10 mg L^{-1}, the recovery rate of fluorides is higher than that of chlorides, consistent with the results at 250 mg L^{-1} and supporting the feasibility of the proposed application at lower target concentrations. Instead, when all the ions are simultaneously present in solution at a concentration of 50 mg L^{-1} each, there is minimal difference in the recovery rate of the different monovalent anions. However, the recovery of sulfates is strongly reduced, while the recovery rate of phosphates is slightly lower than that of fluorides and chlorides. While recovery rate provides insight into the overall efficiency of the recovery process, these metrics do not provide information regarding the selectivity of the fGO membranes. To address this, selectivity coefficients were calculated (Table S2), proving moderate selectivity towards both monovalent and divalent anions in single-ion solutions. However, when all the anions were simultaneously present, the fGO membrane exhibited no selectivity towards monovalent anions, whereas moderate selectivity towards sulfates and phosphates was observed.

3.3 | Cleanroom Waste Reutilization

The real case study was conducted using a 250 ml sample of wastewater collected in the cleanroom (www.piquetlab.it) of the National Metrology Institute of Italy (INRiM). The sample was collected from the waste of diluted hydrofluoric acid used for wafer etching. The sample was neutralized using $Ca(OH)_2$ in order to precipitate CaF_2. The solution became immediately turbid and was left to rest overnight at ambient temperature. The neutralization via $Ca(OH)_2$ addition played a dual role: it initiated the precipitation of CaF_2 and simultaneously triggered the gelation of dissolved silicon species. For this reason, the lower part of the solution, containing the CaF_2 precipitate, was collected and subsequently filtered through a PES membrane to recover the precipitate (Figure 5a). The rest of the solution, containing the suspension of polymerized silica and calcium silicate complexes, was purified using a secondary PES membrane. This ensured that the remaining filtrate to be treated by the fGO membranes was substantially free of silicon, thereby preventing co-precipitation in the final recovery stage.

The solution was then filtered through an fGO membrane to recover the remaining fluorides. A 10 ml NaOH 0.1 M stripping solution was used to collect and concentrate the fluorides. The feed and stripping solutions were alternately filtered 3 times each. This process was then repeated on the same membrane using 5 different feed and stripping solutions, all sourced from the same batches. It is important to note that this fGO membrane, after fabrication, was protected with a layer of PES on the top, thus creating a stacked PES-fGO-PES structure. This was done to prevent the mechanical damage that was observed on unprotected membranes after several filtering processes, mainly due to the weakening of the fGO structure caused by the action of NaOH and the physical impact of pouring the feed solutions inside the apparatus, directly

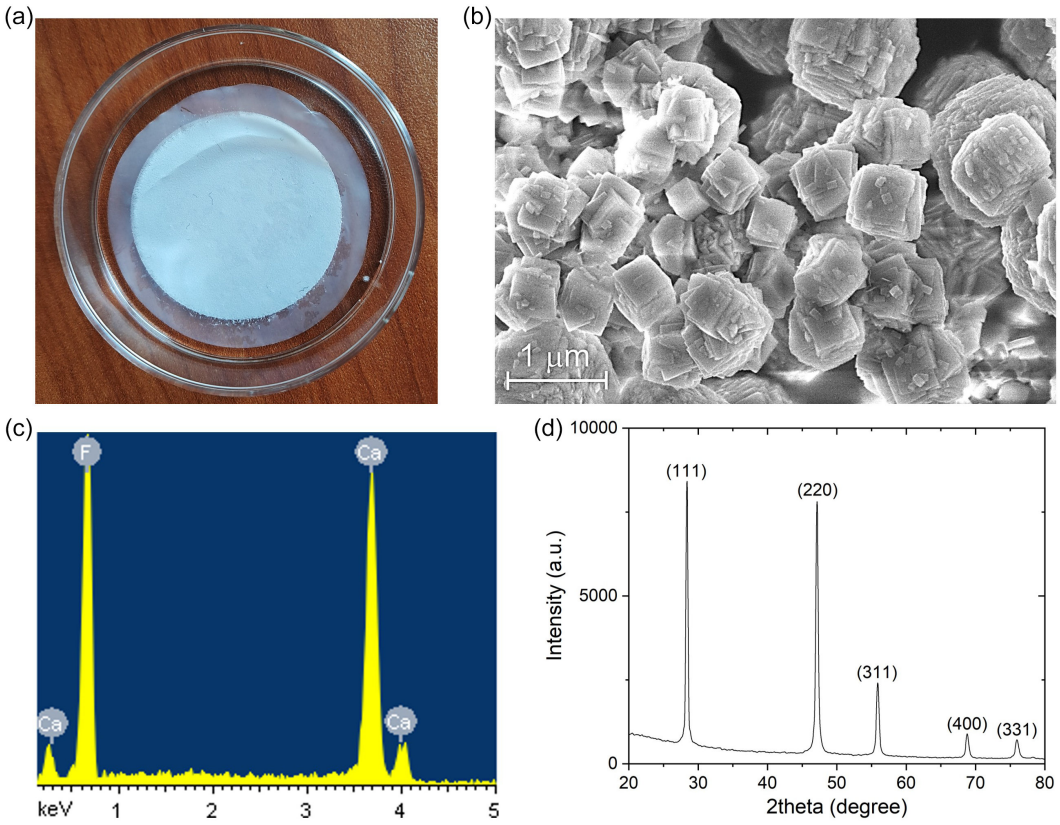

FIGURE 5 | (a) PES membrane with white CaF_2 precipitate. (b) FESEM image of CaF_2 precipitate. The cubic structure is clearly visible. (c) EDX spectrum of CaF_2 precipitate, confirming the presence of calcium and fluorine only. (d) XRD spectrum of CaF_2 precipitate, confirming the crystalline structure of pure fluorite.

26999412, 2026, 9, Downloaded from https://advanced.onlinelibrary.wiley.com/doi/10.1002/aesr.70255 by Iit Istituti Italiano Di Tecnologia, Wiley Online Library on [07/09/2026]. See the Terms and Conditions (https://onlinelibrary.wiley.com/terms-and-conditions) on Wiley Online Library for rules of use; OA articles are governed by the applicable Creative Commons License

onto the membrane surface. The PES-fGO-PES stack successfully prevented this damage without affecting the water flux.

At the end of the tests, the stripping solution had a concentration of F^- of 20.8 mg L^{-1}. At this point, a solution of $Ca(OH)_2$ 1 g L^{-1} was added to the stripping solution, with the added volume being 4% of the stripping solution's total volume. This increased the CaF_2 concentration to more than double its solubility limit (approximately 41 mg L^{-1}), causing the precipitation of the salt. The stripping solution was filtered through a PES membrane to recover the precipitate.

Both the initial precipitate and the latter were inspected using FESEM. The typical cubic crystal structure of CaF_2 was observed (Figure 5b). The size of the crystals ranged from hundreds of nanometers to few micrometers. EDX spectra reported the presence of only calcium and fluorine, in an atomic ratio of 1:2 (Figure 5c). XRD analysis confirmed that the precipitate is pure CaF_2, thanks to the presence of the (111), (220), (311), (400), and (331) peaks, observed at 28.4°, 47.1°, 55.9°, 68.8°, and 76.0°, respectively (Figure 5d). High-resolution ICP-MS was used to confirm the results of EDX and XRD. The main impurities detected in the recovered CaF_2 salt were Si, Na, Al, and Sr, with concentrations of 270 ± 35, 82 ± 19, 64.2 ± 6.0, and 54.63 ± 0.98 mg kg^{-1}, respectively. Lower levels were observed for Fe (9.35 ± 0.15 mg kg^{-1}), Ba (3.45 ± 0.06 mg kg^{-1}), Sb (2.6 ± 1.8 mg kg^{-1}), Li (2.13 ± 0.66 mg kg^{-1}), and Ni (1.41 ± 0.37 mg kg^{-1}). Trace amounts in the order of μg kg^{-1} of Pb, Cr, Mn, Cd, Bi, V, and Co were also measured, whereas Cu, Se, and As were below the quantifiable level under the adopted analytical conditions. Overall, the impurity profile was dominated by Si, followed by Na, Al, Sr, and Fe, while potentially toxic elements such as Cd, Pb, As, and Co were present only at trace or non-quantifiable levels.

The high elemental purity and stoichiometric consistency observed across these analyses suggest that the recovered material meets the stringent requirements of acid-grade fluorspar (>97% CaF_2), which is the primary precursor for HF production in the semiconductor industry.

At the end of this first set of filtrations, the concentration of fluorine in the wastewater was almost halved, passing from 21 mg L^{-1} down to 11 mg L^{-1}, while contemporaneously recovering CaF_2 as a solid product. At this concentration, the wastewater did not meet the requirements for discharge or for drinking water (1.5 mg L^{-1} for EU and 4.0 mg L^{-1} for USA). Therefore, further steps of filtration were performed.

We simulated a multistage filtration system by preparing fresh fGO membranes and using them to further treat the wastewater, following the filtration protocol previously described. After a second filtration step, the concentration of fluorine was further lowered to 4 mg L^{-1}, confirming the behavior initially obtained for the fGO membranes. This result is already sufficient to satisfy the USA requirement. A third filtration step allowed us to push down the concentration further to 1.4 mg L^{-1}, achieving the goal of 1.5 mg L^{-1} required by the EU regulation. Taking into account the entire multi-stage process, 94% of the remaining fluoride was removed, with 33% recovered as solid CaF_2. The comprehensive mass balance is provided in Table S3.

4 | Conclusion

This study successfully investigated a membrane made of functionalized graphene oxide (fGO) for the purification of cleanroom wastewater and the recovery of calcium fluoride (CaF_2). fGO was obtained through a novel and green approach. Comprehensive characterization of the membrane confirmed the effectiveness of the functionalization procedure. The selectivity of fGO membranes towards fluorides was tested using different solutions at different concentrations. The results showed a higher uptake of fluorides at all concentrations. However, in the presence of competing anions (especially monovalent), the selectivity drops drastically, suggesting that their optimal use is as a targeted polishing step for fluoride-rich industrial streams.

This targeted application was validated using real cleanroom wastewater through a process combining initial chemical precipitation, followed by a multi-stage membrane process. Initial neutralization with calcium hydroxide precipitated the bulk fluoride fraction, which was filtered to recover CaF_2. The solution containing the remaining dissolved fraction, which escapes standard precipitation treatment due to the solubility limit of CaF_2, was subsequently filtered using fGO membranes. The fluorine removed from the wastewater was concentrated and precipitated in the form of a CaF_2 fine powder. The fGO membranes showed stable performance, retaining approximately 94% of the remaining fluorine ions within 3 filtration steps and allowing for a recovery of 33% of that target fluoride fraction as solid CaF_2. The final permeate met the standards for drinkable water, as defined by USA and EU regulations.

Compared to conventional purely extractive technologies, such as standard reverse osmosis, activated alumina, or ion exchange resins, this closed-loop configuration provides a distinct quantitative advantage by concurrently satisfying stringent regulatory discharge limits and facilitating resource circularity without generating a secondary brine disposal problem. By converting an industrial effluent into a source of recovered critical raw materials and compliant discharge water, this work establishes a bench-scale feasibility framework for circular water management in the semiconductor sector. Future research will focus on enhancing ion-specific selectivity in multi-anion solutions, evaluating the long-term stability of these membranes systematically, optimizing the flux considering the trade-off between permeability and selectivity of these membranes, and transitioning this multi-stage batch process into a continuous automated system.

Acknowledgments

The authors wish to express their gratitude to Dr. Roberto Rocci for providing the cleanroom wastewater.

Funding

This work was supported by the European Union - NextGenerationEU under the National Recovery and Resilience Plan (NRRP), Mission 04 Component 2 Investment 3.1 Project Code: IR0000027 CUP: B33C22000710006 iENTRANCE@ENL: Infrastructure for EnergyTRAnsition aNd Circular Economy@EuroNanoLab.

26999412, 2026, 9, Downloaded from https://advanced.onlinelibrary.wiley.com/doi/10.1002/aesr.70255 by Iit Istituti Italiano Di Tecnologia, Wiley Online Library on [07/09/2026]. See the Terms and Conditions (https://onlinelibrary.wiley.com/terms-and-conditions) on Wiley Online Library for rules of use; OA articles are governed by the applicable Creative Commons License

Conflicts of Interest

The authors declare no conflicts of interest.

Data Availability Statement

The data that support the findings of this study are available from the corresponding author upon reasonable request.

References

1. European Commission, [Online], accessed May 19, 2025, https://single-market-economy.ec.europa.eu/sectors/raw-materials/areas-specific-interest/critical-raw-materials_en.

2. European Commission, Communication From the Commission to the European Parliament, the Council, the European Economic and Social Committee and the Committee of the Regions Tackling the Challenges in Commodity Markets and on Raw Materials (European Commission, 2017).

3. European Commission, On the 2017 List of Critical Raw Materials for the EU (European Commission, 2017).

4. European Commission, Critical Raw Materials Resilience: Charting a Path Towards Greater Security and Sustainability (European Commission, 2020).

5. European Commission, Study on the Critical Raw Materials for the EU. 2023 – Final Report (Publications Office of the European Union, 2023).

6. European Parliament and Council of the European Union, Directive (EU) Drinking Water Directive 2020/2184, Official Journal of the European Union 435 (2020), 1–62.

7. R. Epsztein, "Intrinsic Limitations of Nanofiltration Membranes to Achieve Precise Selectivity in Water-Based Separations," *Frontiers in Membrane Science and Technology* 1 (2022): 1048416.

8. N. Maroufi and N. Hajilary, "Nanofiltration Membranes Types and Application in Water Treatment: A Review," *Sustainable Water Resources Management* 9, no. 5 (2023): 142.

9. Y.-C. An, X.-X. Gao, W.-L. Jiang, et al., "A Critical Review on Graphene Oxide Membrane for Industrial Wastewater Treatment," *Environmental Research* 223 (2023): 115409.

10. J. Ma, D. Ping, and X. Dong, "Recent Developments of Graphene Oxide-Based Membranes: A Review," *Membranes* 7 (2017): 7030052.

11. A. Aixalà-Perello, A. Pedico, M. Laurenti, et al., "Scalable and Highly Selective Graphene-Based Ion-Exchange Membranes With Tunable Permselectivity," *npj 2D Materials and Applications* 7 (2023): 46.

12. J. Abraham, K. S. Vasu, C. D. Williams, et al., "Tunable Sieving of Ions Using Graphene Oxide Membranes," *Nature Nanotechnology* 12 (2017): 546–550.

13. A. Pedico, L. Baudino, A. Aixalà-Perello, and A. Lamberti, "Green Methods for the Fabrication of Graphene Oxide Membranes: From Graphite to Membranes," *Membranes* 13 (2023): 429.

14. International Energy Agency, Water-Energy Nexus (International Energy Agency, 2017).

15. L. Baudino, A. Pedico, S. Bianco, M. Periolatto, C. F. Pirri, and A. Lamberti, "Crown-Ether Functionalized Graphene Oxide Membrane for Lithium Recovery From Water," *Membranes* 12 (2022): 233.

16. T.-N. Kim, H. Kim, C. Kim, and J. Hwang, "Swelling-Resistant Graphene Oxide Membranes Reinforced by Heteroatomic Inorganic Dots for Electrochemical Lithium Recovery From Aqueous Solution," *Desalination* 592 (2024): 118089.

17. S. Liu, X. Tong, L. Huang, et al., "Lithium-Ion Extraction Using Electro-Driven Freestanding Graphene Oxide Composite Membranes," *Journal of Membrane Science* 672 (2023): 121448.

18. J. Zhang, N. Chen, P. Su, and C. Feng, "Fluoride Removal From Aqueous Solution by Zirconium-Chitosan/Graphene Oxide Membrane," *Reactive and Functional Polymers* 114 (2017): 127–135.

19. S. Kanrar, S. Debnath, P. De, et al., "Preparation, Characterization and Evaluation of Fluoride Adsorption Efficiency From Water of Iron-Aluminium Oxide-Graphene Oxide Composite Material," *Chemical Engineering Journal* 306 (2016): 269–279.

20. A. Pedico, S. Bocchini, E. Tresso, and A. Lamberti, "Enhanced Capacitive Deionization Exploiting Novel Functionalized Graphene Oxide Electrodes," *Advanced Materials Technologies* 7 (2022): 2101513.

21. B. D. Ossonon and D. Bélanger, "Synthesis and Characterization of Sulfophenyl-Functionalized Reduced Graphene Oxide Sheets," *RSC Advances* 7, no. 44 (2017): 27224–27234.

22. A. Gholampour, M. V. Kiamahalleh, D. N. H. Tran, T. Ozbakkaloglu, and D. Losic, "From Graphene Oxide to Reduced Graphene Oxide: Impact on the Physiochemical and Mechanical Properties of Graphene–Cement Composites," *ACS Applied Materials & Interfaces* 9, no. 49 (2017): 43275–43286.

23. M. D. Frogley, C. Wang, G. Cinque, and A. H. Barber, "Polarised Infrared Microspectroscopy of Edge-Oriented Graphene Oxide Papers," *Vibrational Spectroscopy* 75 (2014): 178–183.

24. K. Haubner, J. Murawski, P. Olk, et al., "The Route to Functional Graphene Oxide," *ChemPhysChem* 11 (2010): 2131–2139.

25. C. Xu, R.-s. Yuan, and X. Wang, "Selective Reduction of Graphene Oxide," *New Carbon Materials* 29 (2014): 61–66.

26. Z. Khan and N. Sekar, "Comparing the Linear and Non-Linear Optical Properties of Keto-Enol Forms of N-Alkyl, N-Aryl, and O-Alkyl Substituted 2-Hydroxybenzophenone," *Computational and Theoretical Chemistry* 1242 (2024): 114980.

27. Z. Ciplak, N. Yildiz, and A. Calimli, "Investigation of Graphene/Ag Nanocomposites Synthesis Parameters for Two Different Synthesis Methods," *Fullerenes, Nanotubes and Carbon Nanostructures* 23 (2015): 361–370.

28. H. Kim, B. S. Lee, Y. Lee, J. K. Lee, and I. S. Choi, "Solid-Phase Extraction of Nerve Agent Degradation Products Using Poly[(2-(meth-acryloyloxy)ethyl)trimethylammonium Chloride] Thin Films," *Talanta* 197 (2019): 500–508.

29. K. M. Aujara, B. W. Chieng, N. A. Ibrahim, N. Zainuddin, and C. T. Ratnam, "Gamma-Irradiation Induced Functionalization of Graphene Oxide With Organosilanes," *International Journal of Molecular Science* 20 (2019): 1910.

30. K. N. Kudin, B. Ozbas, H. C. Schniepp, R. K. Prud'homme, I. A. Aksay, and R. Car, "Raman Spectra of Graphite Oxide and Functionalized Graphene Sheets," *Nano Letters*, 8, no. 1 (2007): 36–41.

31. J. Yu, Y. Wang, Y. He, et al., "Calcium Ion-Sodium Alginate Double Cross-Linked Graphene Oxide Nanofiltration Membrane With Enhanced Stability for Efficient Separation of Dyes," *Separation and Purification Technology* 276 (2021): 119348.

32. P. Su, F. Wang, Z. Li, C. Y. Tang, and W. Li, "Graphene Oxide Membranes: Controlling Their Transport Pathways," *Journal of Materials Chemistry A* 8 (2020): 15319–15340.

Supporting Information

Additional supporting information can be found online in the Supporting Information section.

26999412, 2026, 9, Downloaded from https://advanced.onlinelibrary.wiley.com/doi/10.1002/aesr.70255 by Iit Istituti Italiano Di Tecnologia, Wiley Online Library on [07/09/2026]. See the Terms and Conditions (https://onlinelibrary.wiley.com/terms-and-conditions) on Wiley Online Library for rules of use; OA articles are governed by the applicable Creative Commons License